

INTERPRETATION OF NEURAL NETWORKS IS SUSCEPTIBLE TO UNIVERSAL ADVERSARIAL PERTURBATIONS

Haniyeh Ehsani Oskouie

Farzan Farnia

Sharif University of Technology
Department of Computer Engineering
hehsani@ce.sharif.edu

The Chinese University of Hong Kong
Department of Computer Science & Engineering
farnia@cse.cuhk.edu.hk

ABSTRACT

Interpreting neural network classifiers using gradient-based saliency maps has been extensively studied in the deep learning literature. While the existing algorithms manage to achieve satisfactory performance in application to standard image recognition datasets, recent works demonstrate the vulnerability of widely-used gradient-based interpretation schemes to norm-bounded perturbations adversarially designed for every individual input sample. However, such adversarial perturbations are commonly designed using the knowledge of an input sample, and hence perform sub-optimally in application to an unknown or constantly changing data point. In this paper, we show the existence of a *Universal Perturbation for Interpretation (UPI)* for standard image datasets, which can alter a gradient-based feature map of neural networks over a significant fraction of test samples. To design such a UPI, we propose a gradient-based optimization method as well as a principal component analysis (PCA)-based approach to compute a UPI which can effectively alter a neural network's gradient-based interpretation on different samples. We support the proposed UPI approaches by presenting several numerical results of their successful applications to standard image datasets.

Index Terms— Explainable Deep Learning, Adversarial Attacks, Universal Adversarial Perturbations

1. INTRODUCTION

Deep neural networks (DNNs) have attained impressive results in many computer vision [1], speech processing [2], and computational biology [3] problems. While DNNs usually achieve state-of-the-art performance in application to image and speech datasets, their performance is highly vulnerable to minor perturbations adversarially designed for an input sample [4, 5]. Recently, it has been shown that not only do adversarial perturbations alter the prediction of DNN machines, but further one can design small norm-bounded perturbations to significantly change the gradient-based feature maps used for interpreting the prediction of neural networks [6, 7]. Understanding the mechanisms behind such adversarial attacks has received significant attention in the recent machine learning literature.

Similar to standard adversarial attacks, the adversarial perturbations targeting the gradient-based interpretation of DNNs are commonly designed separately for every input sample, which requires full knowledge of the input data point. However, the input sample can constantly alter in several adversarial attack scenarios, and it may not be computationally feasible to optimize different perturbations for a continuously-changing input data point. Furthermore, in several real-world adversarial attack scenarios, the input features are hidden in test time, and therefore the adversary has no or little infor-

mation of the target input sample. In these adversarial attack problems, the adversary can still design and apply a universal adversarial perturbation (UAP) [8] to alter the gradient-based interpretation for a typical input sample. While several UAP attack schemes [8–16] have been proposed to target the prediction of neural networks in the context of classification, the current deep learning literature lacks universal attack schemes that target the gradient-based interpretation of neural networks.

In this paper, we focus on designing *Universal Perturbations for Interpretation (UPI)* as universal attacks aimed to change the saliency maps of neural nets over a significant fraction of input data. To achieve this goal, we formulate an optimization problem to find a UPI perturbation with the maximum impact on the total change in the gradient-based feature maps over the training samples. We propose a projected gradient method called UPI-Grad for solving the formulated optimization problem. Furthermore, in order to handle the difficult non-convex nature of the formulated optimization problem, we develop a principal component analysis (PCA)-based approach called UPI-PCA to approximate the solution to this problem using the top singular vector of fast gradient method (FGM) perturbations to the interpretation vectors. We demonstrate that the spectral UPI-PCA scheme yields the first-order approximation of the solution to the UPI-Grad optimization problem.

To implement the UPI-PCA scheme for generating universal perturbations, we propose a stochastic optimization method which can efficiently converge to the top singular vector of first-order interpretation-targeting perturbations. Finally, we demonstrate our numerical results of applying the UPI-Grad and UPI-PCA methods to standard image recognition datasets and neural network architectures. Our numerical results reveal the vulnerability of commonly-used gradient-based feature maps to universal perturbations which can significantly alter the interpretation of neural networks. The empirical results show the satisfactory convergence of the proposed stochastic optimization method to the top singular vector of the attack scheme, and further indicate the proper generalization of the designed attack vector to test samples unseen during the optimization of the universal perturbation. We can summarize the contributions of this work as follows:

- Extending universal adversarial attacks to alter gradient-based interpretations of neural networks,
- Proposing the gradient-based UPI-Grad method to design universal perturbations for the neural nets' interpretation,
- Developing the spectral UPI-PCA method for optimizing universal perturbations to the interpretation of neural networks,
- Providing numerical evidence on the sensitivity of the interpretation of neural networks to universal perturbations.

2. PRELIMINARIES

2.1. Interpretation methods

In this section, we review standard gradient-based interpretation mechanisms for deep neural network classifiers and explain the notation and definitions used in the paper. Throughout the paper, we use notation $X \in \mathcal{X} \subseteq \mathbb{R}^d$ to denote the random vector of input features and notation $Y \in \mathcal{Y} = \{1, 2, \dots, k\}$ to denote a k -ary random label which the neural network classifier aims to predict. Here, the goal of the deep neural network learner is to find a function $f \in \mathcal{F}_{\text{nn}}$ from neural net space \mathcal{F}_{nn} which can accurately predict Y from an observation of X . To do this, we apply the standard empirical risk minimization (ERM) approach which minimizes the empirical expected loss $\mathbb{E}[\ell(f(X), Y)]$ over training samples $(x_i, y_i)_{i=1}^n$ and loss function $\ell(y, \hat{y})$ between predicted label \hat{y} and actual label y .

For the interpretation of a trained neural net $f(x)$ at an input $x \in \mathbb{R}^d$, we use feature importance maps as an explanation of the classifier f 's prediction. Given the neural net's prediction $c \in \mathcal{Y}$ for the input x (the label with the maximum prediction score), we use $S_c(x)$, to denote the output of the f final layer's neuron corresponding to label c . Here, we briefly review two widely-used gradient-based interpretation schemes for generating a feature importance map, which we later use in our numerical analysis.

- **Simple gradient method:** As introduced in [17] and further analyzed in [18] for deep neural network classifiers, the simple gradient method is based on a first-order linear approximation of the classifier neural network's output and is defined as the following normalized gradient vector:

$$I_{\text{SG}}(x) := \frac{\nabla_x S_c(x)}{\|\nabla_x S_c(x)\|_1} \quad (1)$$

In the above, $\|\cdot\|_1$ denotes the ℓ_1 -norm, i.e. the summation of the absolute value of an input vector's entries.

- **Integrated gradients method:** As introduced in [6], the feature importance map of the integrated gradient method is defined as the ℓ_1 -normalized version of the following score:

$$I_{\text{IG}}^{\text{unorm}}(x) := \frac{\Delta x}{M} \sum_{k=1}^M \nabla_x S_c(x^0 + \frac{k}{M} \Delta x),$$

$$I_{\text{IG}}(x) = \frac{I_{\text{IG}}^{\text{unorm}}(x)}{\|I_{\text{IG}}^{\text{unorm}}(x)\|_1} \quad (2)$$

In this definition, M is the number of intermediate points between a reference point x^0 and input x , and $\Delta x = x - x^0$ is the difference between the input and reference points.

2.2. Adversarial Attacks and Universal Perturbations

Given a neural network function f , an ϵ -norm-bounded adversarial perturbation is a vector δ satisfying $\|\delta\| \leq \epsilon$ which maximizes the classification loss function in an ϵ distance from an input (x, y) , i.e. the solution to the following optimization problem:

$$\max_{\delta: \|\delta\| \leq \epsilon} \ell(y, f(x + \delta)). \quad (3)$$

[6] extends the concept of an adversarial perturbation to neural networks' interpretations. Here, for an interpretation scheme $I(x)$, the aim is to find a norm-bounded vector $\delta \in \mathbb{R}^d$ that maximizes a distance function $\mathcal{D}(\cdot, \cdot)$ between the original and perturbed data points,

$$\max_{\delta \in \mathbb{R}^d: \|\delta\| \leq \epsilon} \mathcal{D}(I(x), I(x + \delta)). \quad (4)$$

While standard adversarial attacks assign different perturbation vectors to different input data, universal adversarial perturbations (UAPs) introduced in [8] use the same perturbation vector for every input sample. Therefore, UAPs provide a more effective approach to alter neural net predictions for an unknown input. A standard approach for designing classification-based UAPs is to solve the following optimization problem for a set of training data $\{(x_i, y_i)_{i=1}^n\}$:

$$\max_{\delta: \|\delta\| \leq \epsilon} \frac{1}{n} \sum_{i=1}^n \ell(y_i, f(x_i + \delta)). \quad (5)$$

In the above problem, we find a universal perturbation which maximizes the sum of loss values for universally-perturbed data points.

3. UNIVERSAL PERTURBATIONS FOR INTERPRETATION

As discussed in the previous sections, while universal perturbations are extensively studied in the context of classification, the current literature lacks a universal perturbation scheme that targets the neural net's gradient-based interpretation. Such a universal perturbation for the interpretation of neural nets will be useful to target the gradient-based interpretation of a neural network for an unobserved or constantly-updating input sample.

Here, we propose *Universal Perturbations for Interpretation (UPI)* which is a universal attack scheme targeting gradient-based interpretations of deep neural net classifiers. To define the optimization problem for UPI, we propose the following maximization problem for interpretation scheme I and distance measure \mathcal{D} :

$$\begin{aligned} \operatorname{argmax}_{\delta \in \mathbb{R}^d} \quad & \mathbb{E}_{Z \sim \mathcal{N}(\mathbf{0}, \sigma^2 I)} \left[\frac{1}{n} \sum_{i=1}^n \mathcal{D}(I(x_i), I(x_i + \delta + Z)) \right] \\ \text{subject to} \quad & \|\delta\| \leq \epsilon \end{aligned} \quad (6)$$

Here, we search for a norm-bounded perturbation $\delta \in \mathbb{R}^d$ that results in the maximum change in the summation of distances between unperturbed and universally-perturbed interpretations. Note that we define the objective function as the expectation over an additive Gaussian $Z \sim \mathcal{N}(\mathbf{0}, \sigma^2 I)$ with a zero mean and an isotropic covariance matrix $\sigma^2 I$ to smoothen the objective function and address the zero gradient of the distance function at the zero point $\delta = \mathbf{0}$. Note that $\sigma \geq 0$ is a hyperparameter in the UPI framework which we choose to be significantly smaller than $\sigma \ll \epsilon$ in our numerical experiments. To solve the above optimization problem, we propose a projected gradient ascent method described in Algorithm 1.

However, we note that similar to the classification-based universal perturbations, the above optimization problem is in general non-convex and can be significantly challenging as a local search method could get stuck at sub-optimal stationary points due to the existence of multiple locally optimal perturbations. As discussed in [11, 12], a significant challenge in such optimization problems is the symmetric behavior of the objective function around the zero perturbation $\delta = \mathbf{0}$, which can lead to the failure of a gradient-based method in solving the optimization task.

To address this challenge, we propose a variant of the optimization problem in (6), which only concerns finding the optimal perturbation direction. Here, our goal is to find a universal direction $\delta \in \mathbb{R}^d$ which is aligned with the universally-aligned perturbations to input samples. In the following, we design such an optimization problem where the perturbations are all aligned with the universal direction δ while they could have different magnitudes chosen by

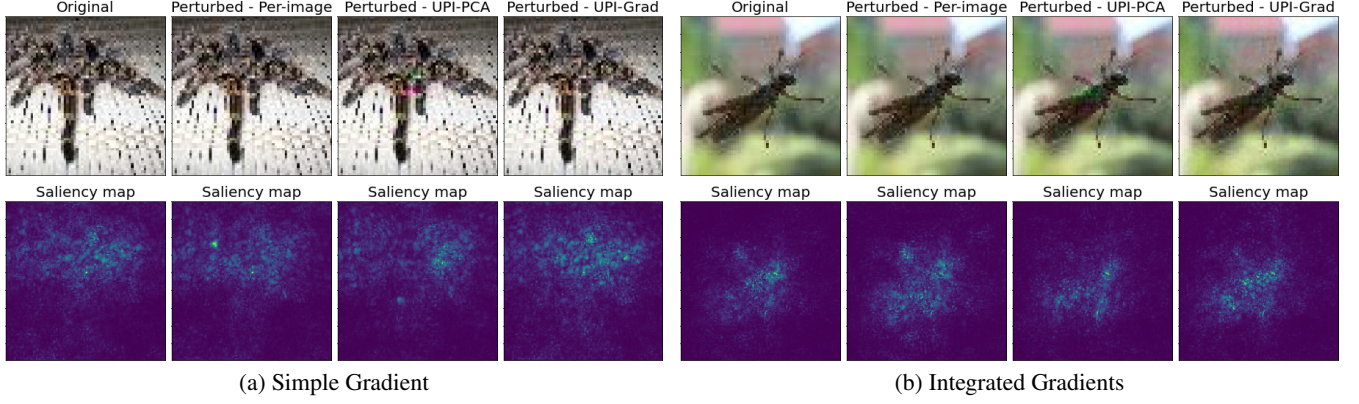


Fig. 1: Interpretation of the VGG-16 networks on two Tiny-ImageNet samples before and after adding the perturbations.

Algorithm 1 UPI-Grad

Input: Training data $(x_i, y_i)_{i=1}^n$, maximum perturbation norm ϵ , feature map $I(\cdot)$, stepsize α , standard deviation σ
Define dissimilarity function $\mathcal{D}(x, x') = \|I(x) - I(x')\|_2^2$
Initialize $\delta = z$ with a normal $z \sim \mathcal{N}(\mathbf{0}, \sigma^2 I)$
for epoch $\in \{1, \dots, N_{ep}\}$ **do**
 for minibatch $B \subset X_{1:n}$ **do**
 Draw normal $z \sim \mathcal{N}(\mathbf{0}, \sigma^2 I)$
 Update $\delta \leftarrow \delta + \frac{\alpha}{|B|} \sum_{x \in B} \nabla_z \mathcal{D}(x, x + z + \delta)$
 Project on the ϵ -norm ball $\delta = \frac{\delta}{\max\{1, \|\delta\|/\epsilon\}}$
 end for
end for
Output: Universal perturbation δ

Algorithm 2 UPI-PCA

Input: Training data $(x_i, y_i)_{i=1}^n$, maximum perturbation norm ϵ , feature map $I(\cdot)$, stepsize α , standard deviation σ
Define dissimilarity function $\mathcal{D}(x, x') = \|I(x) - I(x')\|_2^2$
Initialize $\delta = z$ with a normal $z \sim \mathcal{N}(\mathbf{0}, \sigma^2 I)$
for epoch $\in \{1, \dots, N_{ep}\}$ **do**
 for minibatch $B \subset X_{1:n}$ **do**
 Draw random $z \sim \mathcal{N}(\mathbf{0}, \sigma^2 I)$
 Compute gradients $G = [\nabla_z \mathcal{D}(x, x + z)]_{x \in B}$
 Update $\delta \leftarrow \delta + \frac{\alpha}{|B|} \sum_{i=1}^{|B|} (\delta^\top G_i) G_i$
 Project on the ϵ -norm ball $\delta = \frac{\delta}{\max\{1, \|\delta\|/\epsilon\}}$
 end for
end for
Output: Universal perturbation δ

the sample-based scalar variable c_i 's. We also regularize c_i 's to have a bounded absolute value through the regularization term $-\frac{\lambda}{2} c_i^2$.

$$\begin{aligned} \max_{\delta \in \mathbb{R}^d} \quad & \frac{1}{n} \sum_{i=1}^n \max_{c_i \in \mathbb{R}} \mathbb{E} \left[\mathcal{D}(I(x_i), I(x_i + Z + c_i \delta)) - \frac{\lambda}{2} c_i^2 \right] \\ \text{subject to} \quad & \|\delta\| \leq \epsilon \end{aligned} \quad (7)$$

To have a first-order approximation of the solution to the above problem, we use the following proposition:

Proposition 1. *Consider the objective function in (7). Suppose that every summation term $\mathcal{D}(I(x), I(x + \delta))$ is L -Lipschitz in δ . Then, assuming that $\tau := \frac{L\sqrt{d}\epsilon^2}{\sigma} < \lambda$, for every $\|\delta\|_2 \leq \epsilon$ we will have*

$$\begin{aligned} & \frac{1}{\lambda + \tau} \left(\delta^\top \mathbb{E} [\nabla_z \mathcal{D}(I(x_i), I(x_i + Z))] \right)^2 \\ & \leq \left\{ \max_{c_i \in \mathbb{R}} \mathbb{E} [\mathcal{D}(I(x_i), I(x_i + Z + c_i \delta))] - \frac{\lambda}{2} c_i^2 \right\} \\ & \quad - \mathbb{E} [\mathcal{D}(I(x_i), I(x_i + Z))] \\ & \leq \frac{1}{\lambda - \tau} \left(\delta^\top \mathbb{E} [\nabla_z \mathcal{D}(I(x_i), I(x_i + Z))] \right)^2. \end{aligned}$$

Proof. We defer the proof to the Appendix. \square

Based on the above proposition, we obtain the following opti-

mization problem as the first-order approximation of (7):

$$\begin{aligned} \max_{\delta \in \mathbb{R}^d} \quad & \frac{1}{n} \sum_{i=1}^n \left(\delta^\top \mathbb{E} [\nabla_z \mathcal{D}(I(x_i), I(x_i + Z))] \right)^2 \\ \text{subject to} \quad & \|\delta\| \leq \epsilon \end{aligned} \quad (8)$$

The next proposition reveals that the solution to the above problem is indeed the top singular vector of the first-order gradients of the randomly-perturbed distance function at $\delta = \mathbf{0}$:

Proposition 2. *Consider the optimization problem in Equation (8) for the ℓ_2 -norm case. Then, the solution to the optimization problem is the top right singular vector of the following matrix:*

$$G := \mathbb{E}_{Z \sim \mathcal{N}(\mathbf{0}, \sigma^2 I)} \left[\begin{bmatrix} \nabla_z \mathcal{D}(I(x_1), I(x_1 + Z)) \\ \vdots \\ \nabla_z \mathcal{D}(I(x_n), I(x_n + Z)) \end{bmatrix} \right].$$

Proof. We defer the proof to the Appendix. \square

The above result suggests using the top principal component of the gradient matrix G as the UPI perturbation. Hence, we propose the principal component analysis (PCA)-based UPI-PCA in Algorithm 2 as a stochastic power method for computing the top right singular vector of matrix G .

Table 1: Average dissimilarity of VGG-16, MobileNet, and 2-layer CNN trained on Tiny-ImageNet, CIFAR-10, and MNIST respectively.

Interpretation method	Attack	Type	Tiny-ImageNet		CIFAR-10		MNIST		
			VGG-16	MobileNet	VGG-16	MobileNet	MobileNet	2-layer CNN	2-layer FCN
Simple Gradient	Random	Per image	0.407	0.664	0.275	0.482	0.342	1.012	0.085
		Universal	0.407	0.665	0.274	0.485	0.342	1.006	0.079
	Interpretation	Per image-PGD	0.777	0.783	0.590	0.710	0.566	1.024	0.324
		Per image-FGM	0.772	0.778	0.573	0.705	0.549	0.911	0.334
		UPI-PCA-PGD (Ours)	0.550	0.681	0.350	0.540	0.428	1.501	0.308
		UPI-PCA-FGM (Ours)	0.538	0.668	0.343	0.553	0.428	1.275	0.358
		UPI-Grad (Ours)	0.598	0.719	0.439	0.641	0.441	1.045	0.242
	Classification	Universal	0.540	0.699	0.372	0.587	0.379	1.042	0.185
Integrated Gradients	Random	Per image	0.278	0.528	0.201	0.312	0.240	0.798	0.028
		Universal	0.277	0.528	0.199	0.311	0.241	0.794	0.026
	Interpretation	Per image-PGD	0.749	0.754	0.560	0.652	0.510	0.828	0.246
		Per image-FGM	0.734	0.728	0.531	0.618	0.476	0.768	0.228
		UPI-PCA-PGD (Ours)	0.430	0.578	0.271	0.431	0.318	0.849	0.166
		UPI-PCA-FGM (Ours)	0.434	0.561	0.258	0.490	0.321	0.851	0.166
		UPI-Grad (Ours)	0.531	0.676	0.287	0.541	0.385	0.835	0.183
	Classification	Universal	0.408	0.581	0.280	0.412	0.272	0.824	0.063

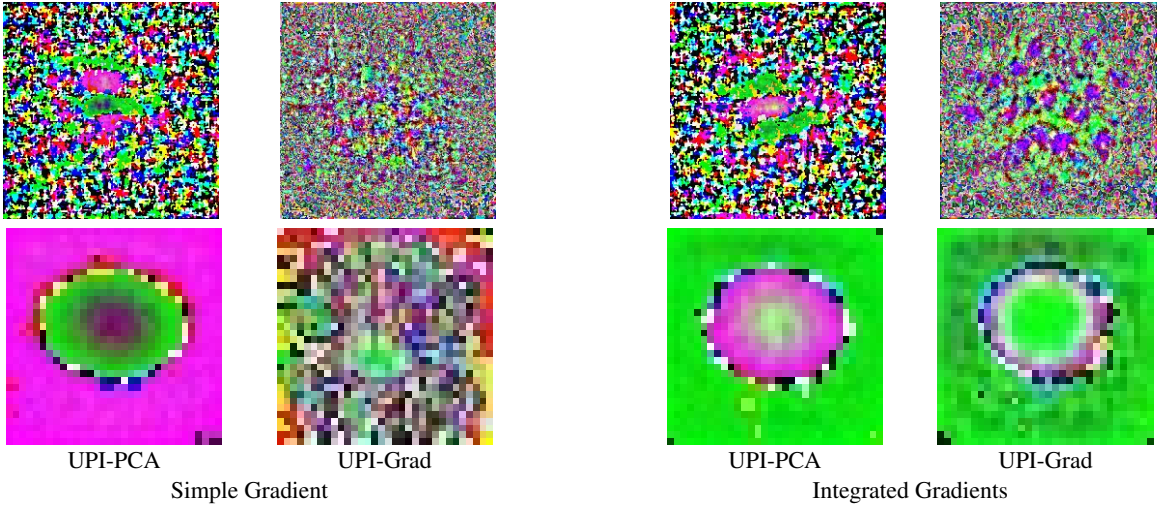


Fig. 2: Visualization of UPI perturbations in VGG-16 experiments. The top and bottom rows are the Tiny-ImageNet and CIFAR-10 UPIs.

4. NUMERICAL RESULTS

We performed numerical experiments to evaluate the proposed UPI schemes on standard image datasets including MNIST [19], CIFAR-10 [20], and Tiny-ImageNet [21]. Note that Tiny-ImageNet is a downsized version of the ImageNet dataset containing 100,000 images from 200 ImageNet classes, with 500 images per class. For universal attacks against feature importance interpretation, we trained VGG-16 [22] and MobileNet [23] models on Tiny-ImageNet and CIFAR-10 datasets. For MNIST, we trained a MobileNet, a simple 2-layer convolution neural net (CNN), and a simple 2-layer fully-connected net (FCN) with the ReLU activation.

In the experiments, we used the following normalized dissimilarity score to evaluate the performance of the perturbations:

$$\mathcal{D}(x, x') := \frac{\|I(x) - I(x')\|_2}{\|I(x)\|_2} \quad (9)$$

where x, x' denote the original and perturbed images, and $I(\cdot)$ is the specified interpretation scheme. We report the mean of the above dissimilarity scores over the test set. All the perturbations were scaled such that the norm value $\epsilon = \frac{1000}{256}$ for Tiny-ImageNet, and $\epsilon = \frac{100}{256}$ for CIFAR-10 and MNIST. Since the resolution of CIFAR-10 and MNIST samples were lower than Tiny-ImageNet, the norm value was chosen to be smaller. We ran all per-image iterative attack algorithms for 150 iterations, and stepsize $\alpha = 0.5$. We evaluated the random attacks 10 times, and report the results with the mean dissimilarity value.

As reported in Table 1, we compared UPIs with several baselines including (i) a normally-distributed random perturbation generated both per-image and universally, (ii) per-image adversarial perturbations on interpretation designed individually for each input image using the PGD method in [6], (iii) classification-based universal adversarial perturbation as described in [24]. We also report the dissim-

ilarity scores for the proposed UPI-Grad and UPI-PCA algorithms.

As Table 1's scores suggest, the UPIs performed significantly better than a random perturbation, but were often a little weaker than per-image adversarial perturbations. In some cases, UPIs even performed as well as per-image adversarial perturbations. In addition, the average dissimilarity of classification-based UAPs is shown in Table 1. While their achieved scores were somewhat inferior to UPI-Grad, they still performed successfully in comparison to random and per-image perturbations. Figure 1 visually shows the effect of the designed perturbations on the interpretations of VGG-16 classifiers. Also, Figure 2 visualizes the designed UPIs for the trained VGG-16-nets and highlights their visual patterns. These empirical results confirm our hypothesis that universal perturbations (both UAPs and UPIs) can significantly change the interpretation of deep neural networks.

5. REFERENCES

- [1] Alex Krizhevsky, Ilya Sutskever, and Geoffrey E Hinton. Imagenet classification with deep convolutional neural networks. *Communications of the ACM*, 60(6):84–90, 2017.
- [2] Li Deng, Geoffrey Hinton, and Brian Kingsbury. New types of deep neural network learning for speech recognition and related applications: An overview. In *2013 IEEE international conference on acoustics, speech and signal processing*, pages 8599–8603. IEEE, 2013.
- [3] Babak Alipanahi, Andrew Delong, Matthew T Weirauch, and Brendan J Frey. Predicting the sequence specificities of dna- and rna-binding proteins by deep learning. *Nature biotechnology*, 33(8):831–838, 2015.
- [4] Christian Szegedy, Wojciech Zaremba, Ilya Sutskever, Joan Bruna, Dumitru Erhan, Ian Goodfellow, and Rob Fergus. Intriguing properties of neural networks. *arXiv preprint arXiv:1312.6199*, 2013.
- [5] Ian J Goodfellow, Jonathon Shlens, and Christian Szegedy. Explaining and harnessing adversarial examples. *arXiv preprint arXiv:1412.6572*, 2014.
- [6] A. Ghorbani, A. Abid, and J. Zou. Interpretation of neural networks is fragile. *Association for the Advancement of Artificial Intelligence*, 2019.
- [7] Juyeon Heo, Sunghwan Joo, and Taesup Moon. Fooling neural network interpretations via adversarial model manipulation. *Advances in Neural Information Processing Systems*, 32, 2019.
- [8] Seyed-Mohsen Moosavi-Dezfooli, Alhussein Fawzi, Omar Fawzi, and Pascal Frossard. Universal adversarial perturbations. In *Proceedings of the IEEE conference on computer vision and pattern recognition*, pages 1765–1773, 2017.
- [9] Omid Poursaeed, Isay Katsman, Bicheng Gao, and Serge Belongie. Generative adversarial perturbations. In *Proceedings of the IEEE Conference on Computer Vision and Pattern Recognition*, pages 4422–4431, 2018.
- [10] Jamie Hayes and George Danezis. Learning universal adversarial perturbations with generative models. In *2018 IEEE Security and Privacy Workshops (SPW)*, pages 43–49. IEEE, 2018.
- [11] Valentin Khruikov and Ivan Oseledets. Art of singular vectors and universal adversarial perturbations. In *Proceedings of the IEEE Conference on Computer Vision and Pattern Recognition*, pages 8562–8570, 2018.
- [12] Amit Deshpande, Sandesh Kamath, and KV Subrahmanyam. Universal adversarial attack using very few test examples. 2019.
- [13] Melika Behjati, Seyed-Mohsen Moosavi-Dezfooli, Mahdieh Soleymani Baghshah, and Pascal Frossard. Universal adversarial attacks on text classifiers. In *ICASSP 2019-2019 IEEE International Conference on Acoustics, Speech and Signal Processing (ICASSP)*, pages 7345–7349. IEEE, 2019.
- [14] Yi Xie, Cong Shi, Zhuohang Li, Jian Liu, Yingying Chen, and Bo Yuan. Real-time, universal, and robust adversarial attacks against speaker recognition systems. In *ICASSP 2020-2020 IEEE international conference on acoustics, speech and signal processing (ICASSP)*, pages 1738–1742. IEEE, 2020.
- [15] Weiyi Zhang, Shuning Zhao, Le Liu, Jianmin Li, Xingliang Cheng, Thomas Fang Zheng, and Xiaolin Hu. Attack on practical speaker verification system using universal adversarial perturbations. In *ICASSP 2021-2021 IEEE International Conference on Acoustics, Speech and Signal Processing (ICASSP)*, pages 2575–2579. IEEE, 2021.
- [16] Siao Liu, Zhaoyu Chen, Wei Li, Jiwei Zhu, Jiafeng Wang, Wenqiang Zhang, and Zhongxue Gan. Efficient universal shuffle attack for visual object tracking. In *ICASSP 2022-2022 IEEE International Conference on Acoustics, Speech and Signal Processing (ICASSP)*, pages 2739–2743. IEEE, 2022.
- [17] D. Baehrens, T. Schroeter, S. Harmeling, M. Kawanabe, K. Hansen, and K.-R. MAzller. How to explain individual classification decisions. *Journal of Machine Learning Research*, 11:1803–1831, Jun 2010.
- [18] K. Simonyan, A. Vedaldi, and A. Zisserman. Deep inside convolutional networks: Visualising image classification models and saliency maps. *arXiv preprint arXiv:1312.6034*, 2013.
- [19] Yann LeCun. The mnist database of handwritten digits. <http://yann.lecun.com/exdb/mnist/>, 1998.
- [20] Alex Krizhevsky, Geoffrey Hinton, et al. Learning multiple layers of features from tiny images. 2009.
- [21] J. Deng, W. Dong, R. Socher, L.-J. Li, K. Li, and L. Fei-Fei. ImageNet: A Large-Scale Hierarchical Image Database. In *CVPR09*, 2009.
- [22] Karen Simonyan and Andrew Zisserman. Very deep convolutional networks for large-scale image recognition. *arXiv preprint arXiv:1409.1556*, 2014.
- [23] Andrew G Howard, Menglong Zhu, Bo Chen, Dmitry Kalenichenko, Weijun Wang, Tobias Weyand, Marco Andreetto, and Hartwig Adam. Mobilenets: Efficient convolutional neural networks for mobile vision applications. *arXiv preprint arXiv:1704.04861*, 2017.
- [24] M. Najibi, Z. Xu, J. Dickerson, L. S. Davis, and T. Goldstein. Universal adversarial training. *Association for the Advancement of Artificial Intelligence*, 2020.
- [25] Charles M Stein. Estimation of the mean of a multivariate normal distribution. *The annals of Statistics*, pages 1135–1151, 1981.
- [26] Zinoviy Landsman and Johanna Nešlehová. Stein's lemma for elliptical random vectors. *Journal of Multivariate Analysis*, 99(5):912–927, 2008.

A. PROOFS

A.1. Proof of Proposition 1

To prove this proposition, we first review Stein's lemma [25] from the statistics literature.

Lemma 1 (Stein's lemma [25, 26]). *For every Lipschitz-continuous function $f : \mathbb{R}^d \rightarrow \mathbb{R}$ and isotropic Gaussian vector $Z \sim \mathcal{N}(\mathbf{0}, \sigma^2 I)$, the following equality holds:*

$$\mathbb{E}[\nabla f(x + Z)] = \mathbb{E}\left[\frac{f(x + Z)}{\sigma^2} Z\right].$$

Using Stein's lemma, for every $x, x', y \in \mathbb{R}^d$ we have

$$\begin{aligned} & \|\nabla_x \mathbb{E}[\mathcal{D}(y, x + Z)] - \nabla_x \mathbb{E}[\mathcal{D}(y, x' + Z)]\|_2 \\ &= \|\mathbb{E}[\nabla_x \mathcal{D}(y, x + Z)] - \mathbb{E}[\nabla_x \mathcal{D}(y, x' + Z)]\|_2 \\ &\stackrel{(a)}{=} \left\| \mathbb{E}\left[\frac{Z}{\sigma^2} \mathcal{D}(y, x + Z)\right] - \mathbb{E}\left[\frac{Z}{\sigma^2} \mathcal{D}(y, x' + Z)\right] \right\|_2 \\ &= \left\| \mathbb{E}\left[\frac{Z}{\sigma^2} (\mathcal{D}(y, x + Z) - \mathcal{D}(y, x' + Z))\right] \right\|_2 \\ &\stackrel{(b)}{\leq} \mathbb{E}\left[\left\| \frac{Z}{\sigma^2} (\mathcal{D}(y, x + Z) - \mathcal{D}(y, x' + Z)) \right\|_2\right] \\ &= \mathbb{E}\left[\frac{\|Z\|_2}{\sigma^2} |\mathcal{D}(y, x + Z) - \mathcal{D}(y, x' + Z)|\right] \\ &\stackrel{(c)}{\leq} \mathbb{E}\left[\frac{\|Z\|_2}{\sigma^2} L \|x - x'\|_2\right] \\ &= \frac{L \|x - x'\|_2}{\sigma^2} \mathbb{E}[\|Z\|_2] \\ &\stackrel{(d)}{=} \frac{L \|x - x'\|_2}{\sigma^2} \sqrt{\frac{2d\sigma^2}{\pi}} \\ &\leq \frac{L\sqrt{d}\|x - x'\|_2}{\sigma}. \end{aligned}$$

In the above, (a) follows from Stein's lemma. (b) comes from the application of Jensen's inequality to the convex norm function $\|\cdot\|_2$. (c) is the consequence of the proposition's assumption on the Lipschitz coefficient of \mathcal{D} . (d) uses the analytical solution for the expected value $\mathbb{E}[\|Z\|_2]$ according to $Z \sim \mathcal{N}(\mathbf{0}, \sigma^2 I_{d \times d})$, which is $\sqrt{2d\sigma^2/\pi}$.

Therefore, the gradient of $\mathbb{E}[\mathcal{D}(y, x + Z)]$ with respect to x will be $\frac{L\sqrt{d}}{\sigma}$ -Lipschitz, which means that $\mathbb{E}[\mathcal{D}(y, x + Z)]$ is $\frac{L\sqrt{d}}{\sigma}$ -smooth in x and satisfies the following inequality for every x, x', y :

$$\begin{aligned} & \nabla_x \mathbb{E}[\mathcal{D}(y, x + Z)]^\top (x' - x) - \frac{L\sqrt{d}}{2\sigma} \|x - x'\|_2^2 \\ &\leq \mathbb{E}[\mathcal{D}(y, x' + Z)] - \mathbb{E}[\mathcal{D}(y, x + Z)] \\ &\leq \nabla_x \mathbb{E}[\mathcal{D}(y, x + Z)]^\top (x' - x) + \frac{L\sqrt{d}}{2\sigma} \|x - x'\|_2^2. \end{aligned}$$

As a result, for any $c_i \in \mathbb{R}$ and $x_i, \delta \in \mathbb{R}^d$ the following holds:

$$\begin{aligned} & c_i \nabla_x \mathbb{E}[\mathcal{D}(x_i, x_i + Z)]^\top \delta - \frac{L\sqrt{d}c_i^2}{2\sigma} \|\delta\|_2^2 \\ &\leq \mathbb{E}[\mathcal{D}(x_i, x_i + Z + c_i \delta)] - \mathbb{E}[\mathcal{D}(x_i, x_i + Z)] \\ &\leq c_i \nabla_x \mathbb{E}[\mathcal{D}(x_i, x_i + Z)]^\top \delta + \frac{L\sqrt{d}c_i^2}{2\sigma} \|\delta\|_2^2. \end{aligned}$$

Thus, assuming that $\|\delta\|_2 \leq \epsilon$ and defining $\tau = \frac{L\sqrt{d}\epsilon^2}{\sigma}$, we will have the following inequalities

$$\begin{aligned} & c_i \nabla_x \mathbb{E}[\mathcal{D}(x_i, x_i + Z)]^\top \delta - \frac{\tau}{2} c_i^2 \\ &\leq \mathbb{E}[\mathcal{D}(x_i, x_i + Z + c_i \delta)] - \mathbb{E}[\mathcal{D}(x_i, x_i + Z)] \\ &\leq c_i \nabla_x \mathbb{E}[\mathcal{D}(x_i, x_i + Z)]^\top \delta + \frac{\tau}{2} c_i^2, \end{aligned}$$

which implies that

$$\begin{aligned} & c_i \nabla_x \mathbb{E}[\mathcal{D}(x_i, x_i + Z)]^\top \delta - \frac{\lambda + \tau}{2} c_i^2 \\ &\leq \mathbb{E}[\mathcal{D}(x_i, x_i + Z + c_i \delta)] - \frac{\lambda}{2} c_i^2 - \mathbb{E}[\mathcal{D}(x_i, x_i + Z)] \\ &\leq c_i \nabla_x \mathbb{E}[\mathcal{D}(x_i, x_i + Z)]^\top \delta - \frac{\lambda - \tau}{2} c_i^2. \end{aligned}$$

The assumption $\lambda > \tau$ implies that the above upper and lower bounds are concave quadratic functions of c_i . Therefore, maximizing the sides of the above inequality over $c_i \in \mathbb{R}$ shows that

$$\begin{aligned} & \frac{1}{\lambda + \tau} \left(\delta^\top \mathbb{E}[\nabla_z \mathcal{D}(I(x_i), I(x_i + Z))] \right)^2 \\ &\leq \left\{ \max_{c_i \in \mathbb{R}} \mathbb{E}[\mathcal{D}(I(x_i), I(x_i + Z + c_i \delta))] - \frac{\lambda}{2} c_i^2 \right\} \\ &\quad - \mathbb{E}[\mathcal{D}(I(x_i), I(x_i + Z))] \\ &\leq \frac{1}{\lambda - \tau} \left(\delta^\top \mathbb{E}[\nabla_z \mathcal{D}(I(x_i), I(x_i + Z))] \right)^2, \end{aligned}$$

which completes the proof.

A.2. Proof of Proposition 2

Note that the objective function in the target optimization problem can be written as:

$$\begin{aligned} & \frac{1}{n} \sum_{i=1}^n \left(\delta^\top \mathbb{E}[\nabla_z \mathcal{D}(I(x_i), I(x_i + Z))] \right)^2 \\ &= \frac{1}{n} \sum_{i=1}^n \left[\left(\delta^\top \mathbb{E}[\nabla_z \mathcal{D}(I(x_i), I(x_i + Z))] \right) \right. \\ &\quad \times \left. \left(\mathbb{E}[\nabla_z \mathcal{D}(I(x_i), I(x_i + Z))]^\top \delta \right) \right] \\ &= \frac{1}{n} \sum_{i=1}^n \left[\delta^\top \mathbb{E}[\nabla_z \mathcal{D}(I(x_i), I(x_i + Z))] \right. \\ &\quad \times \left. \mathbb{E}[\nabla_z \mathcal{D}(I(x_i), I(x_i + Z))]^\top \delta \right] \\ &= \delta^\top \left(\frac{1}{n} \sum_{i=1}^n \left[\mathbb{E}[\nabla_z \mathcal{D}(I(x_i), I(x_i + Z))] \right. \right. \\ &\quad \times \left. \left. \mathbb{E}[\nabla_z \mathcal{D}(I(x_i), I(x_i + Z))]^\top \right] \right) \delta \\ &= \delta^\top M \delta \end{aligned}$$

where we define matrix M as

$$M := \frac{1}{n} \sum_{i=1}^n \left[\mathbb{E}[\nabla_z \mathcal{D}(I(x_i), I(x_i + Z))] \mathbb{E}[\nabla_z \mathcal{D}(I(x_i), I(x_i + Z))]^\top \right].$$

Therefore, for the Euclidean norm constraint $\|\cdot\|_2$, the optimal solution δ^* is aligned with the top eigenvector of matrix M . However, note that M satisfies the following identity:

$$M = \frac{1}{n}GG^\top.$$

As a result, δ^* follows from the normalized top right singular vector of matrix G , and the proof is complete.

B. ADDITIONAL NUMERICAL RESULTS

While increasing the value of fooling rates is not our goal in this paper, they are presented in Table 2. Our results demonstrate that even though most UPIs cause a lower fooling rate than per-image perturbations, they have a considerable impact on the interpretations. We further studied the transferability of UPIs on the datasets mentioned above. As shown in Figure 3, 4, 5, UPI-PCA method has superior generalizability over UPI-Grad. Moreover, UPIs that are generated using Integrated Gradients are strongly correlated with their Simple Gradient counterparts. Additionally, our numerical results in Figure 6, 7, 8, 9, 10 suggest that UPIs are visually structured. UAPs are similarly illustrated for a better comparison. Notably, some of the universal adversarial perturbations found for MNIST have number-like representations.

Table 2: Percentage of fooling rates in VGG-16, MobileNet, and 2-layer CNN trained on Tiny-ImageNet, CIFAR-10, and MNIST.

Attack	Type	Tiny-ImageNet		CIFAR-10		MNIST		
		VGG-16	MobileNet	VGG-16	MobileNet	MobileNet	2-layer CNN	2-layer FCN
Random	Per image	1.18	3.61	0.66	1.08	0.08	0.49	0.05
	Universal	1.18	3.94	0.63	1.15	0.06	0.54	0.05
Interpretation (Simple)	Per image-PGD	76.58	92.64	34.11	30.28	5.46	0.66	0.16
	UPI-PCA-PGD (Ours)	5.59	5.03	4.73	4.12	0.24	2.05	0.39
	UPI-PCA-FGM (Ours)	4.46	4.23	4.57	2.98	0.24	2.17	0.45
	UPI-Grad (Ours)	5.32	10.27	2.54	4.78	0.79	0.82	0.51
Interpretation (Integrated)	Per image-PGD	60.33	47.72	25.19	36.28	5.85	6.45	2.58
	UPI-PCA-PGD (Ours)	5.93	5.77	4.62	3.38	0.26	2.17	0.67
	UPI-PCA-FGM (Ours)	5.62	4.63	4.78	4.00	0.26	2.15	0.63
	UPI-Grad (Ours)	7.41	20.48	5.61	5.62	0.77	1.10	0.76

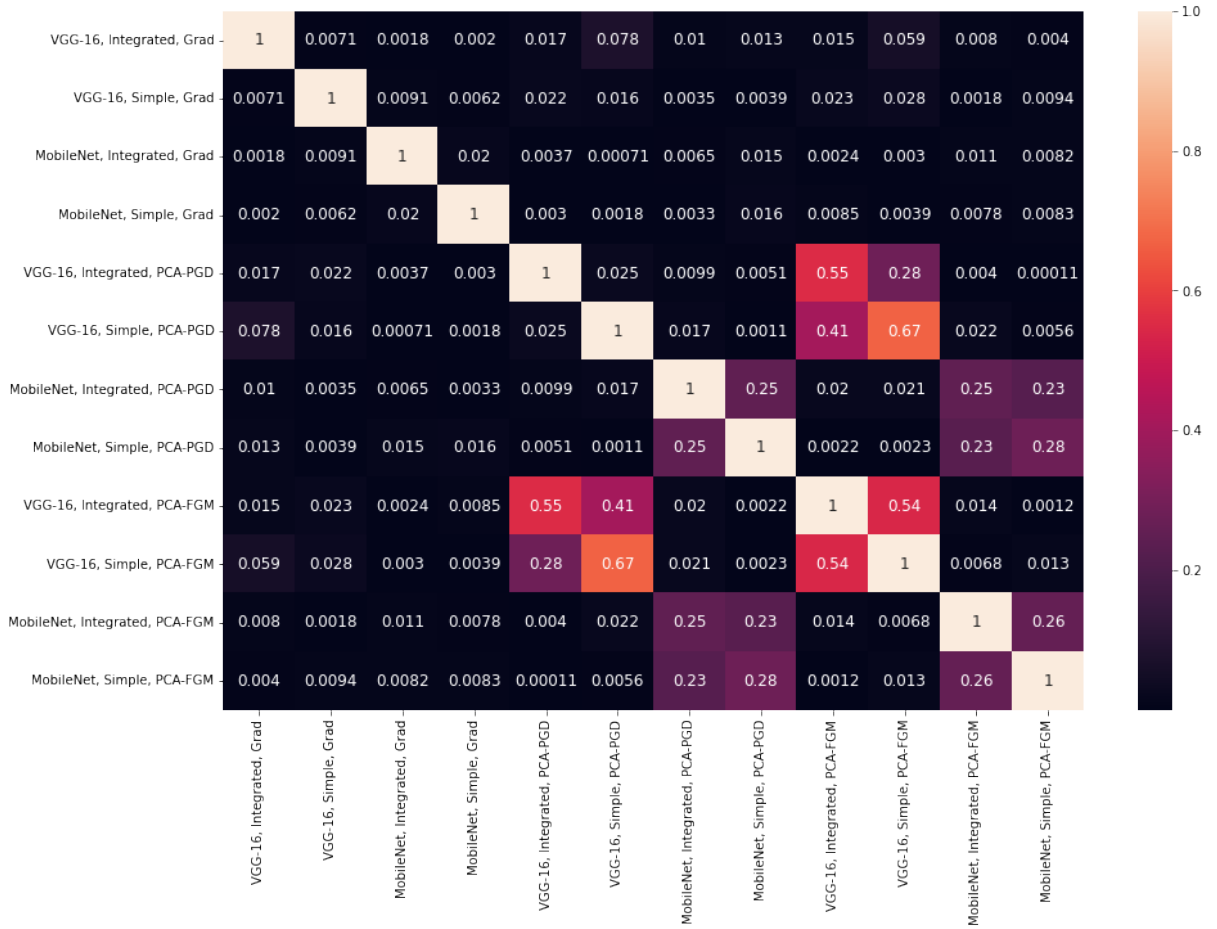


Fig. 3: Cross-correlation between generated UPIs in the Tiny-ImageNet experiments.

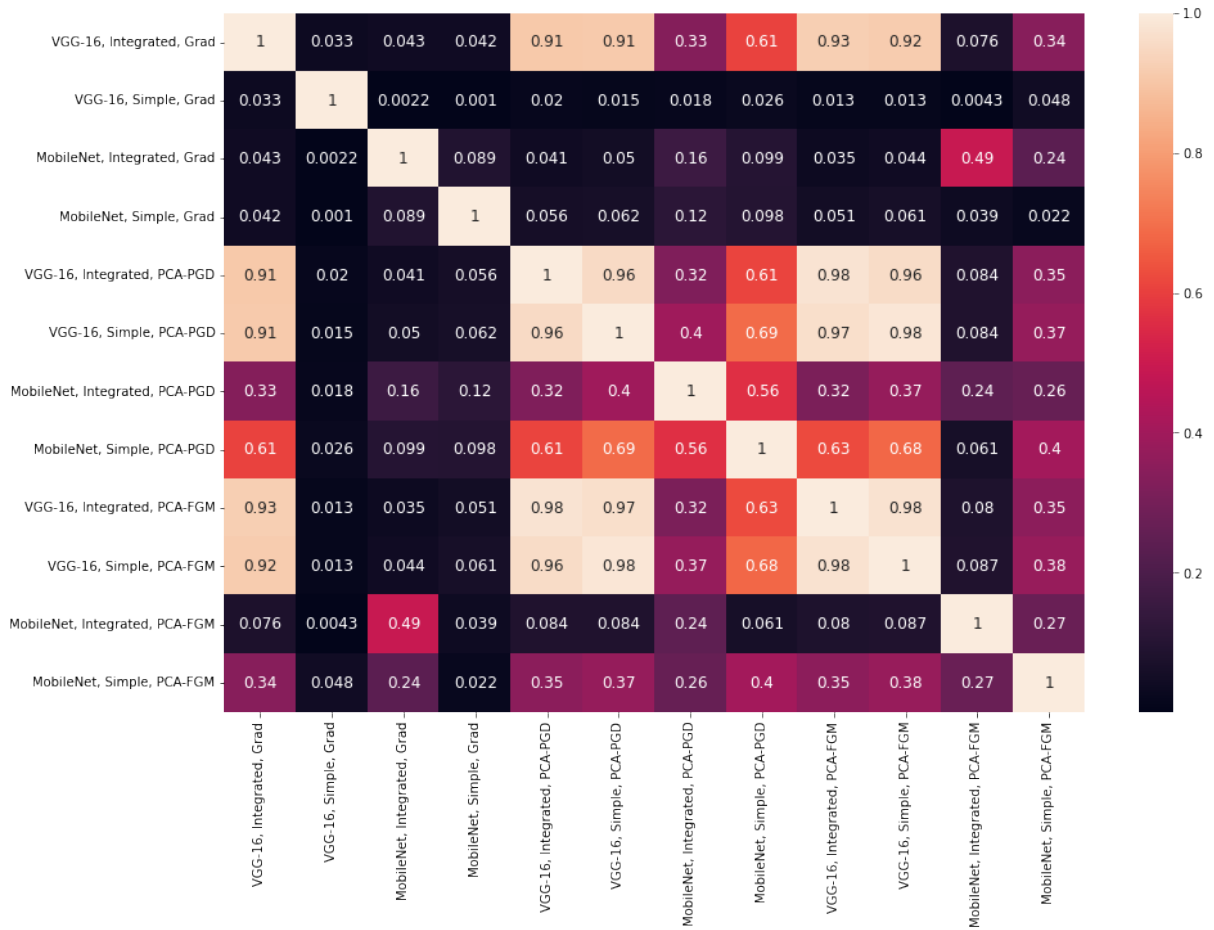
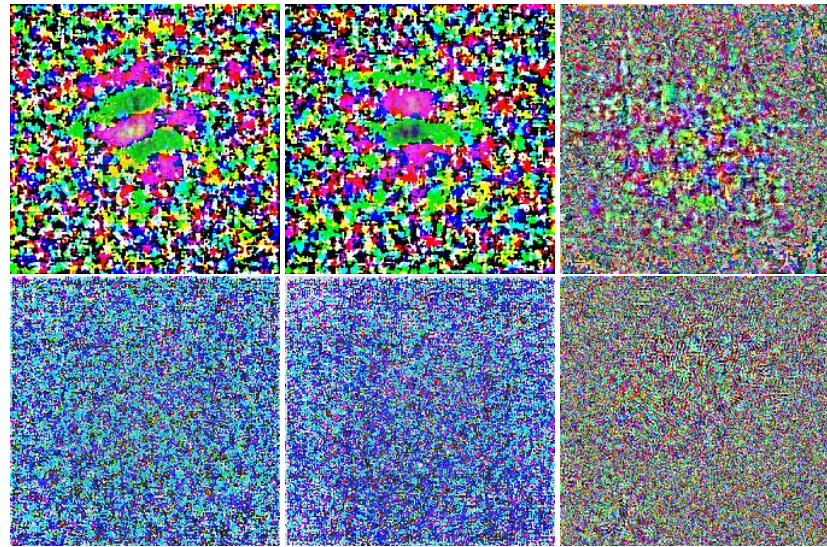


Fig. 4: Cross-correlation between generated UPIs in the CIFAR-10 experiments.



Fig. 5: Cross-correlation between generated UPIs in the MNIST experiments.

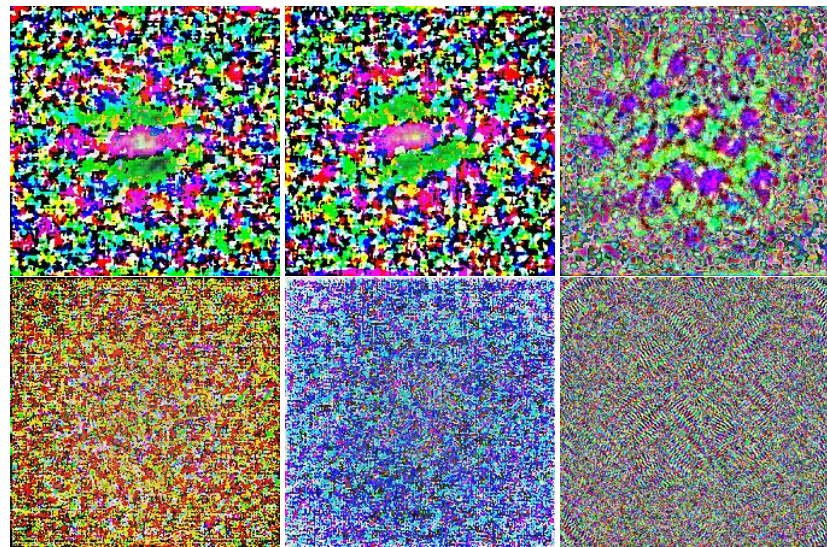


UPI-PCA-PGD

UPI-PCA-FGM

UPI-Grad

(a) Simple Gradient

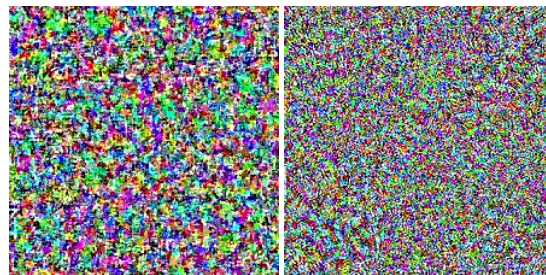


UPI-PCA-PGD

UPI-PCA-FGM

UPI-Grad

(b) Integrated Gradients



VGG-16

MobileNet

(c) UAP

Fig. 6: Univesal perturbations for Tiny-ImageNet. The top and bottom rows of groups (a) and (b) are optimized for VGG-16 and MobileNet, respectively.

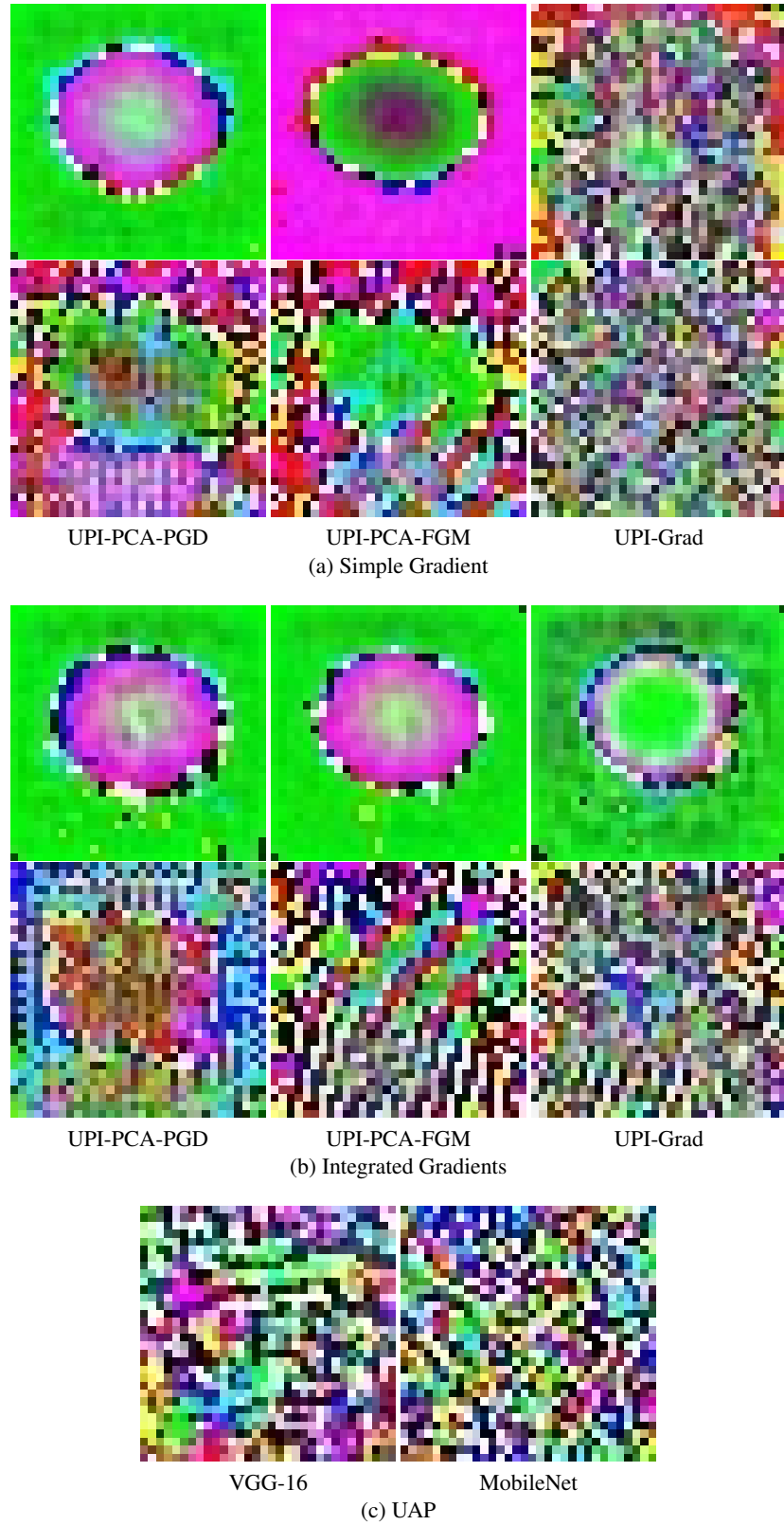


Fig. 7: Universal perturbations for CIFAR-10 data. The top and bottom rows of groups (a) and (b) are optimized for VGG-16 and MobileNet, respectively.

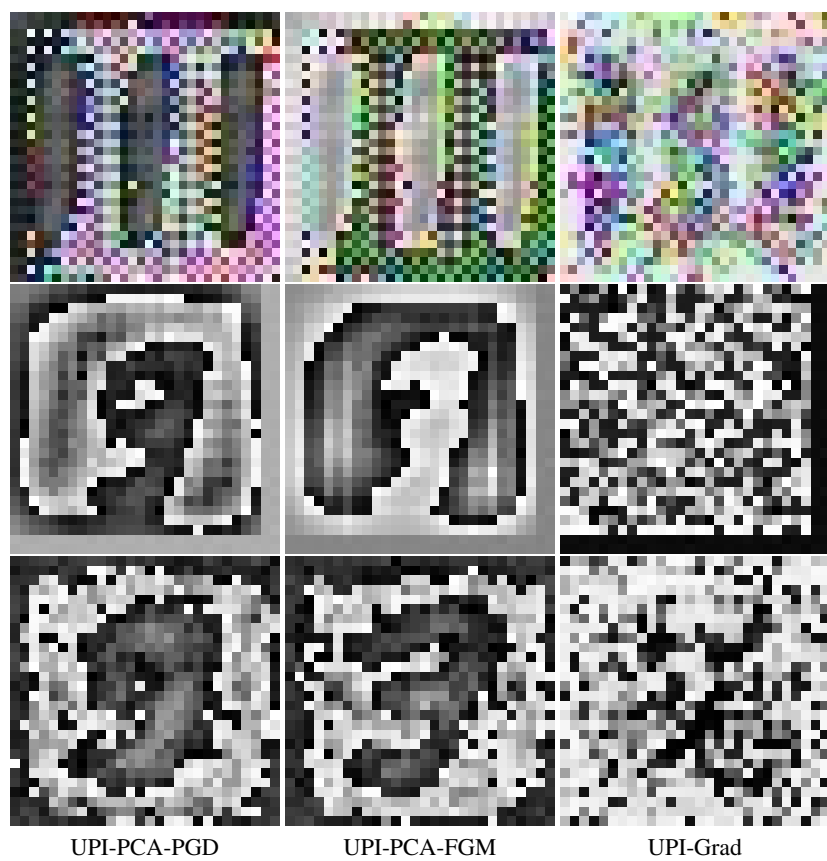


Fig. 8: UPIs using Simple Gradient on MNIST. The top, middle, and bottom rows are found for MobileNet, 2-layer CNN, and 2-layer FCN respectively.

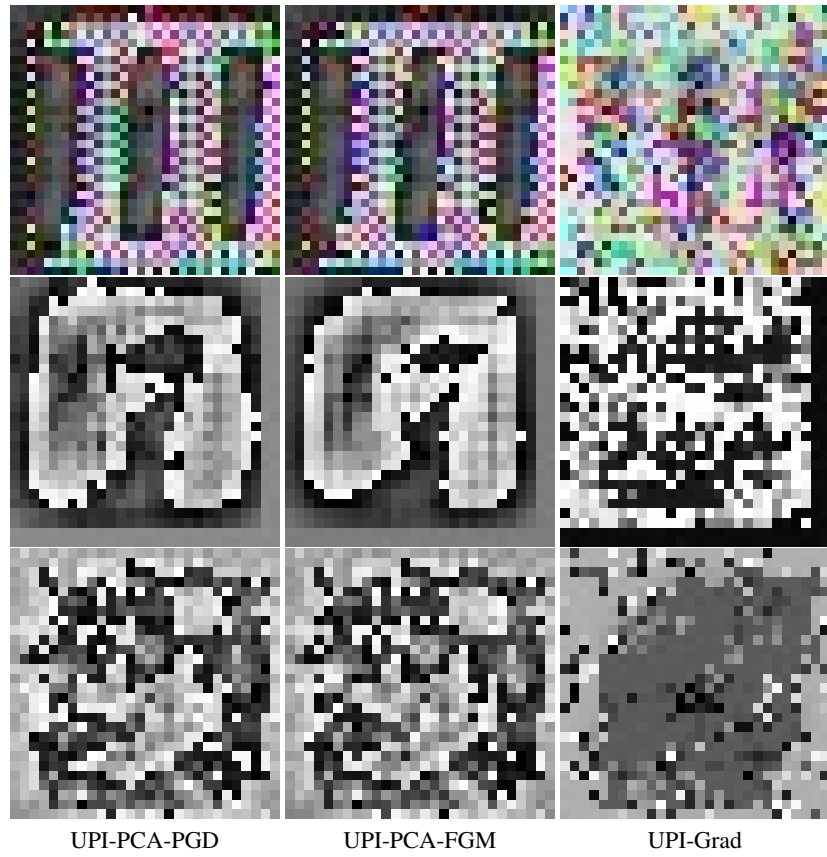


Fig. 9: UPIs designed for Integrated Gradients on MNIST data. The top, middle, and bottom rows are optimized for MobileNet, 2-layer CNN, and 2-layer FCN respectively.

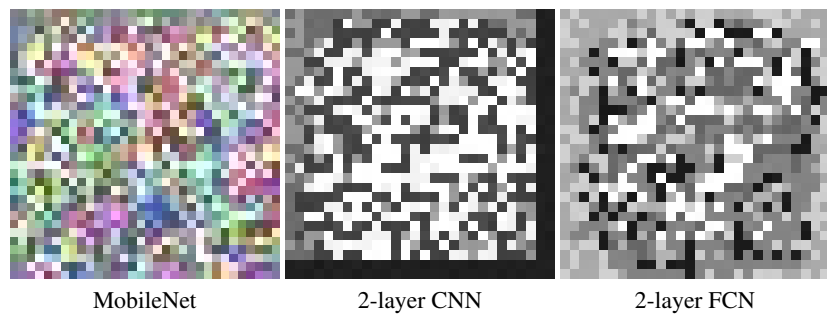


Fig. 10: UAPs optimized for the MNIST data.